Master's Thesis

석 사 학 위 논 문

Convolutional Neural Network for Functional Near-Infrared Spectroscopy-Based Brain-Computer Interface

Thanawin Trakoolwilaiwan (타나윈)

Department of Information and Communication Engineering

정보통신융합공학전공

DGIST

2017

Master's Thesis
석 사 학 위 논 문

Convolutional Neural Network for Functional Near-Infrared Spectroscopy-Based Brain-Computer Interface

Thanawin Trakoolwilaiwan (타나윈)

Department of Information and Communication Engineering

정보통신융합공학전공

DGIST

2017

Convolutional Neural Network for Functional Near-Infrared Spectroscopy-Based Brain-Computer Interface

Advisor: Prof. Ji-Woong Choi
Co-advisor: Prof. Kijoon Lee

by

Thanawin Trakoolwilaiwan
Department of Information and Communication Engineering
DGIST

A thesis submitted to the faculty of DGIST in partial fulfillment of the requirements for the degree of Master of Science in the Department of Information and Communication Engineering. The study was conducted in accordance with Code of Research Ethic[1].

May 12, 2017

Approved by

Professor Ji-Woong Choi   _____
(Advisor)

Professor Kijoon Lee   _____
(Co-advisor)

---

[1] Declaration of Ethical Conduct in Research: I, as a graduate student of DGIST, hereby declare that I have not committed any act that may damage the credibility of my research. These include, but are not limited to: falsification, thesis written by someone else, distortion of research findings or plagiarism. I affirm that my thesis contains honest conclusions based on my own careful research under the guidance of my thesis advisor.

Convolutional Neural Network for Functional Near-Infrared Spectroscopy-Based Brain-Computer Interface

Thanawin Trakoolwilaiwan

Accepted in partial fulfillment of the requirements for the degree of Master of Science.

May 12, 2017

Head of Committee   _____   (signature)
Prof. Ji-Woong Choi

Committee Member   _____   (signature)
Prof. Kijoon Lee

Committee Member   _____   (signature)
Prof. Taesup Moon

Abstract

Brain-computer interface (BCI) is a communication system that translates the brain signal directly to a computer or external devices. It is a promising solution for the patients with neurological disorders as the system is able to restore the movement ability. Various neuroimaging modalities have been utilized for brain signal acquisition, however, functional near-infrared spectroscopy (fNIRS) provides many advantages over other modalities. Hence, it has gained attention for implementing in BCI system. For developing BCI system, the appropriate machine learning algorithm and discriminating features from the hemodynamic response signal are desired, as the previous studies have reported the performance enhancement of fNIRS-based BCI in terms of classification accuracy by focusing on the classifier as well as signal features. The aim of this thesis is to improve the classification accuracy in fNIRS-based BCI by classifying and extracting feature automatically. The convolutional neural network (CNN) was applied owing to the automatic feature extractor and classifier instead of manual feature extraction in the conventional methods. In the experiment, four healthy subjects were measured the hemodynamic response signal evoked by performing tasks including rest, right and left hand motor executions. The conventional methods of fNIRS-based BCI using signal mean, slope, peak, variance, skewness, and kurtosis as the features, and support vector machine (SVM) and artificial neural network (ANN) as the classification methods were compared with CNN-based method. The results show the improvement of classification accuracy of CNN-based method over SVM-based and ANN-based method 6.92% and 3.75%, respectively. The main contributions of this thesis are (1) the promising feature extraction and classification method for fNIRS-based BCI using CNN and (2) the analysis of the feature extracted by conventional methods and convolutional filter of the CNN.

Keywords: Functional near-infrared spectroscopy, brain-computer interface, convolutional neural network, support vector machine, artificial neural network, feature extraction.

Contents

List of Tables

List of Figures

I. INTRODUCTION

1. Motivation

A brain-computer interface (BCI) is the system allows communication pathway between subject and external devices by translating neural activity into the actions of devices using only thought. BCIs can be achieved by measuring and interpreting brain signal from the subject. [1–8]. The process of BCI comprised of (1) brain signal acquisition using neuroimaging modality, (2) signal processing and feature extraction, (3) interpretation of subject's intention by translating signal features, and (4) sending output command to control external devices. The overall process of BCI system is shown in Fig. **1.1**. The design of BCI is helpful for the patients with severe motor disability to improve their quality of life. The achievements of BCI in the clinical applications have been reported for the post-stroke patients [9, 10], amyotrophic lateral sclerosis (ALS) [11, 12], or spinal cord injury (SCI) [13, 14] to control external devices.
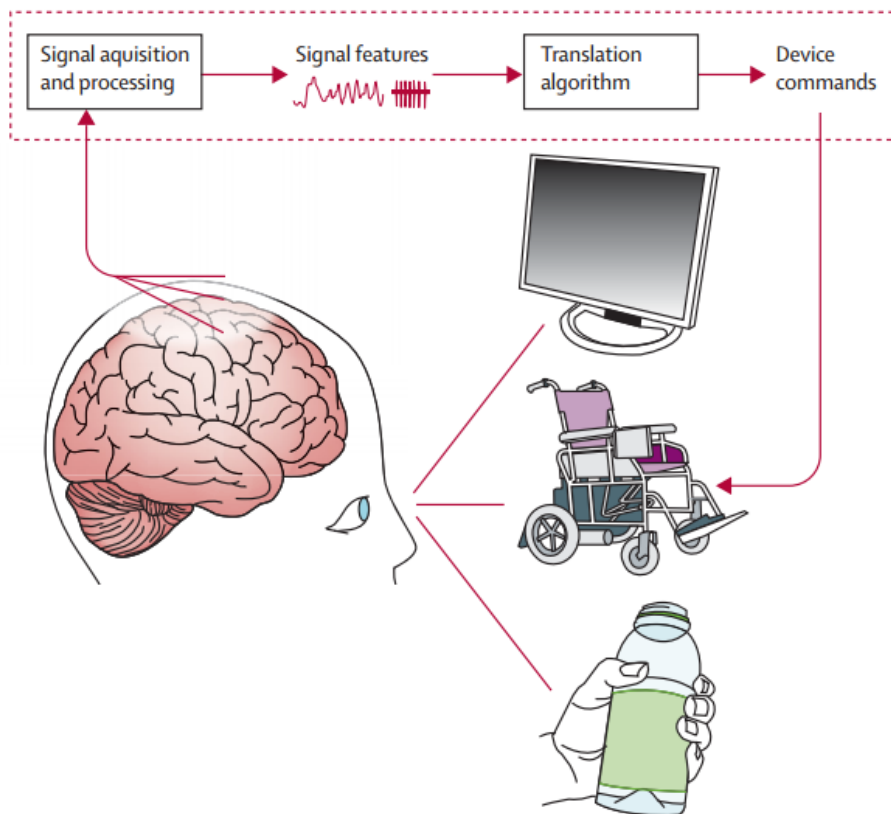
Figure 1.1. Schematic of BCI system (taken from [1])

For brain signal acquisition, various invasive and non-invasive neuroimaging modalities have been applied in the BCI system including, electroencephalography (EEG) [13, 15–19], magnetoencephalography (MEG) [9, 20], electrocorticography (ECoG) [21, 22], functional magnetic resonance imaging (fMRI) [23–25], and functional near-infrared spectroscopy (fNIRS) [10, 11, 14, 15, 26–31]. In spite of the fact that the invasive measurements have benefit on the signal quality, yet high risk due to the surgery is the critical issue. From this reason, non-invasive techniques are widely used in BCI system.

Among the non-invasive modalities, EEG is the most famous in developing BCI applications as a consequence of its high temporal resolution, low cost, and portability, and numerous studies have reported the success of EEG-based BCI. However, the major drawbacks of EEG are low spatial resolution, high sensitivity to head movement and electrical noise interference. On the other hand, fNIRS, as a promising tool for brain signal acquisition in BCI system, offers moderate temporal and spatial resolution, portability and robustness to noise. Consequently, in this thesis, fNIRS was utilized for brain signal acquisition.

In addition, an fNIRS-based BCI is a promising solution for the patients with severe motor disabilities as emerging tool and its advantages over other neuroimaging modalities. Most of the BCI studies rely on improving the classification accuracy, since it is crucial and vital for the safety reason. The previous fNIRS-based BCI studies have proposed various approaches to improve classification accuracy, however, many factors can affect to the accuracy when using conventional methods. Therefore, in this thesis, the proposed method is provided in order to improve performance of fNIRS-based BCI in terms of classification accuracy compared with conventional methods.

2. Objective

The previous studies reported that the convolutional neural network (CNN) have successfully achieved in many applications such as image recognition [32,33], artificial intelligence [34,35], and speech recognition [36], because CNN has ability to learn and generalize the important features from the training data. Thereby, it is reasonable that CNN may be able to enhance performance of fNIRS-based BCI. In this thesis, CNN was utilized to classify and extract features

automatically from the hemodynamic response signal.

The aim of this thesis is to investigate two research questions: (1) can CNN outperform conventional methods in fNIRS-based BCI in terms of classification accuracy? In order to pursue this question, the classification accuracy of performing feature extraction and classification by CNN was compared with the conventional methods in fNIRS-based BCI [37]. (2) how does CNN outperform the conventional methods? The second question was investigated by the analysis of the feature visualization.

The chapters of this thesis are separated into five parts: introduction in Chapter I, background and related work in Chapter II, method in Chapter III, results and discussions in Chapter IV, and conclusion in Chapter V. Chapter II introduces the basic principle of fNIRS, review of fNIRS-based BCI including feature extraction and classification and evaluation method. Chapter III describes the experimental procedure, signal preprocessing and classification, and feature visualization. Chapter IV discuss about the results obtained from the conventional and proposed scheme as well as the future work. The conclusion is given in Chapter V.

II. BACKGROUND AND RELATED WORK

1.   Functional Near-Infrared Spectroscopy (fNIRS)

The fNIRS has been introduced as a novel non-invasive neuroimaging technique to measure hemodynamic response throughout the past few decades. The change in hemoglobin during brain activation in the cerebral cortex caused by neurovascular coupling leads the increase of oxygenated hemoglobin (HbO) and decrease in deoxygenated hemoglobin (HbR) as shown in Fig. **2.1(a)**. The increment of oxygen metabolism, cerebral blood flow (CBF), and cerebral blood volume (CBV) due to neural firing cause the changes of hemoglobin in the cerebral cortex (see Fig. **2.1(b)**).

The fNIRS utilizes light sources to transmit light with near-infrared wavelength (600~900 nm), and then receivers measures the light reflected from the cerebral cortex, in which the light passes through scalp, tissue, and skull to reach the brain [38–40]. The purely absorption or attenuation of the light in medium with known optical path length, homogeneous absorption coefficient, and non-scattering of light, is described by Beer-Lambert law. However, in fact, the biological tissues in the brain are highly scattering, unable to reflect true path length, and
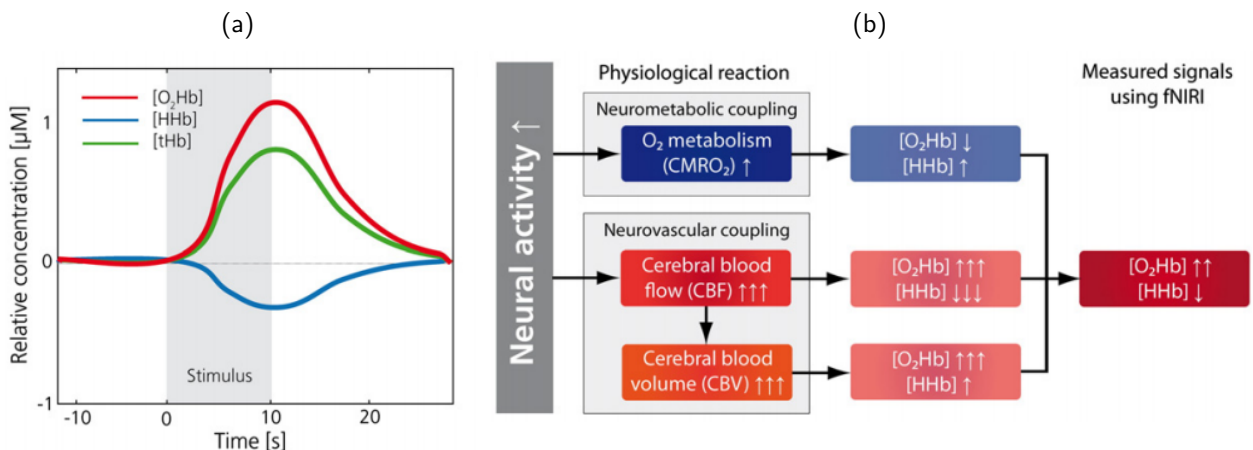
Figure 2.1. Physiological response of hemodynamic signal (taken from [38]). (a) concentration changes of HbO, HbR, and total hemoglobin represented by red, blue, and green lines, respectively. Stimulus period is presented in gray block. (b) Physiological reaction of oxygen metabolism, cerebral blood flow and volume, and concentration changes of HbO and HbR during task stimulus.

absorbed by different compounds. A modified Beer-Lambert law (MBLL) has been developed by assuming that the tissues are homogeneous, constant scattering, and known optical path length. As HbO and HbR have different absorption coefficients in near-infrared wavelength, the relationship between light attenuation due to absorption and scattering and the changes of HbO and HbR concentration can be expressed by MBLL [27, 38, 39].

2.   fNIRS-based BCI

Currently, fNIRS has gained attention in BCI research as an emerging tool for brain signal acquisition. The experiments in fNIRS-based BCI have been conducted in the various tasks including mental arithmetic [27, 28], mental rotation [41], motor imagery [26, 27, 29, 31], and motor execution [15, 28, 29, 42]. The results demonstrated the feasibility of using fNIRS in BCI applications owing to its classification accuracy.

To design the appropriate BCI system, numerous factors must be considered such as accuracy, speed, and ease of use. As the primary aim of BCI is to predict subject intention, misclassification can be a serious cause for unexpected accidents, thus improving accuracy is the most essential part that needed to be concerned [43, 44]. Consequently, it is mandatory to have appropriate classifier as well as features that accurately represent the variability in the hemodynamic response signal to accomplish high classification accuracy [37].

The previous studies related to fNIRS-based BCI have emphasized the improvement in classification accuracy by investigating on the various combination of signal features as well as the machine learning algorithms [37]. In the feature extraction process, statistical properties from time-domain signal [37] and filter coefficients from discrete wavelet transform [45, 46] have been reported. In the classification part, various machine learning algorithms such as linear discriminant analysis (LDA) [15, 26–28, 43, 47], support vector machine (SVM) [11, 29, 48], hidden markov model (HMM) [29], and artificial neural network (ANN) [49] have been successfully implemented in fNIRS-based BCI.

Among the mentioned techniques for fNIRS-based BCI, ANN has been reported as the classifier that achieved the highest performance [50]. Additionally, for feature extraction, most of the studies relied on the statistical properties from time-domain signal. However, it has been

discussed that approaching the high classification accuracy varies based on various factors such as selecting the best features combination [50], size of time window [27], and classification method. Accordingly, appropriate techniques for feature extraction and classification play an important role in fNIRS-based BCI. Herein, a method to overcome the limitation of conventional method was investigated.

3. Feature Extraction and Classification

This section introduces the commonly used features in fNIRS-based BCI, machine learning algorithms (i.e. SVM, ANN, and CNN), and how to evaluate the performance of the classification model in BCI system.

3.1   Feature Extraction

Numerous numbers of fNIRS-based BCI studies have extracted various features from the hemodynamic response signal, while the commonly used features are the statistical properties of the signal in time-domain: signal mean, variance, kurtosis, skewness, peak, and slope, where such features are computed as [37]

$$\mu = \frac{1}{N}\sum_{i=1}^{N} x_i, \tag{2.1}$$

$$\sigma^2 = \frac{\sum_{i=1}^{N}(x_i - \mu)^2}{N}, \tag{2.2}$$

$$K = \frac{\sum_{i=1}^{N}(x_i - \mu)^4/N}{\sigma^4}, \tag{2.3}$$

and

$$S = \frac{\sum_{i=1}^{N}(x_i - \mu)^3/N}{\sigma^3}, \tag{2.4}$$

where μ is signal mean, σ^2 is variance, K kurtosis, S is skewness, N is the total number of samples, x_i represents the concentration changes of HbO and HbR data at i^{th} in the time series data. The signal peak is calculated by selecting the maximum value of the input data, and the slope is computed by using linear regression. The descriptions of the commonly used features

in fNIRS-based BCI: signal mean, slope, variance, peak, skewness, and kurtosis, are provided in Table **2.1**.

3.2 Support Vector Machine (SVM)

The SVM is a discriminative classifier which is able to optimize a separating hyperplane by maximizing the margin [29, 48, 51, 52]. The support vectors are the points which are nearest to the separating hyperplane. Figure **2.2** illustrates the separating hyperplane and support vectors. The separating hyperplane is obtained by

$$min(\frac{1}{2}\|\mathbf{w}\|^2) + C\sum_{i=1}^{L}\varepsilon_i \qquad s.t. \qquad y_i(\mathbf{x}_i \cdot \mathbf{w} + b) - 1 + \varepsilon_i \geq 0, \qquad (2.5)$$

where $\mathbf{w}$ is the weight vector, C is the regularization parameter which is greater than or equal to zero. In order to avoid overfitting issue, proper hyperparameter C is needed to determine throughout the training process. ε_i is the training error which is greater than or equal to zero. $\mathbf{x}_i$ and y_i are input and the class label for the ith sample. b is the bias value.

3.3 Artificial Neural Network (ANN)

An ANN is a non-linear classifier, inspired by the neurons in the human brain, which has capacity of pattern recognition [53]. In general, ANN consists of multiple layers including input layer, fully connected layer (or hidden layer), and output layer, each of which layer contains one or more neurons (see Fig. **2.3**). The training process of ANN is comprised of forward

Table **2.1**. The commonly used features of the hemodynamic response signal in fNIRS-based BCI.

Feature	Description
Mean	Average value of signal amplitude within the window
Slope	Value describes the direction and steepness of the line
Peak	Maximum value of signal amplitude within the window
Variance	Expectation value of the squared deviation or how far the data is spread out
Skewness	Value describes the asymmetry
Kurtosis	Value describes the sharpness of the peak

propagation and backpropagation. The output is estimated through the forward propagation based on the activation function as described by

$$
a_j^l =
\begin{cases}
f(\sum_i w_{ji}^l x_i) & \text{if } l = 2 \\
\\
f(\sum_i w_{ji}^l a_j^{l-1}) & \text{if } l > 2
\end{cases}
\tag{2.6}
$$

where a_j^l is defined as the activation of the jth neuron of the lth layer. w_{ji}^l is denoted as the weight for the connection from j^{th} neuron in the lth layer, to the ith neuron in the $(l-1)^{th}$ layer. x_0 and a_0^l are bias value. x_i is the input data which is used to compute a_j^2 in the second layer. The activation from the previous layer, $(l-1)^{th}$, is used as the input for the lth layer.

Through the forward propagation, the weight values are initialized for the first iteration. To improve the classification performance of the neural network, weight initialization is one of the important factors [54]. Afterward, the weight values are updated throughout backpropagation to minimize the error between output values from the forward propagation and the desired output. The iteration is performed until approaching the minimum loss based on gradient descend learning.

In order to obtain effective model of ANN, various hyperparameters such as learning rate, batch size, and number of epochs should be considered. The learning rate is the parameter to control how fast the weight values can be updated during the training process. The cost function
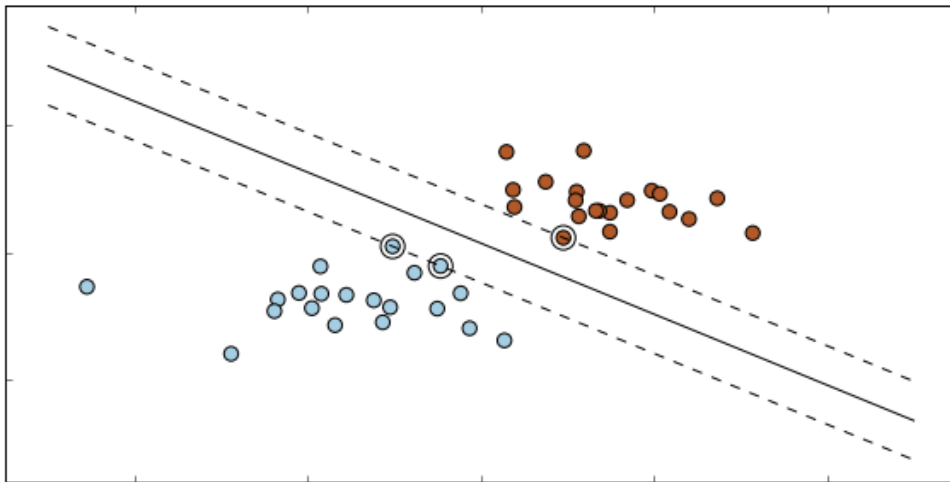
Figure 2.2. SVM in binary classification. The optimal hyperplane (solid line) is obtained by maximizing the distance between support vectors (circled points) or margin (dot lines).

does not converge to a minimum point if the learning rate is too high, while it converges slowly if the learning rate is too low. Additionally, the cost function can converge faster by using batch training. In the batch learning technique, the data are divided into several sets with identical number of sample followed by propagating through the forward propagation and backpropagation, where the batch size is the number of samples in each set [54]. Epoch is defined as the total number of times to complete the training procedure.

3.4 Convolutional Neural Network (CNN)

The CNN is a classification technique inspired by the visual cortex. The CNN is one of the powerful techniques in deep learning because of its capability of learning and generalizing the appropriate features from the input data automatically. The training process in the CNN optimizes the weight parameters of each filter through forward propagation and backpropagation [55]. The structure of CNN contains input layer, convolutional layer, subsampling layer,
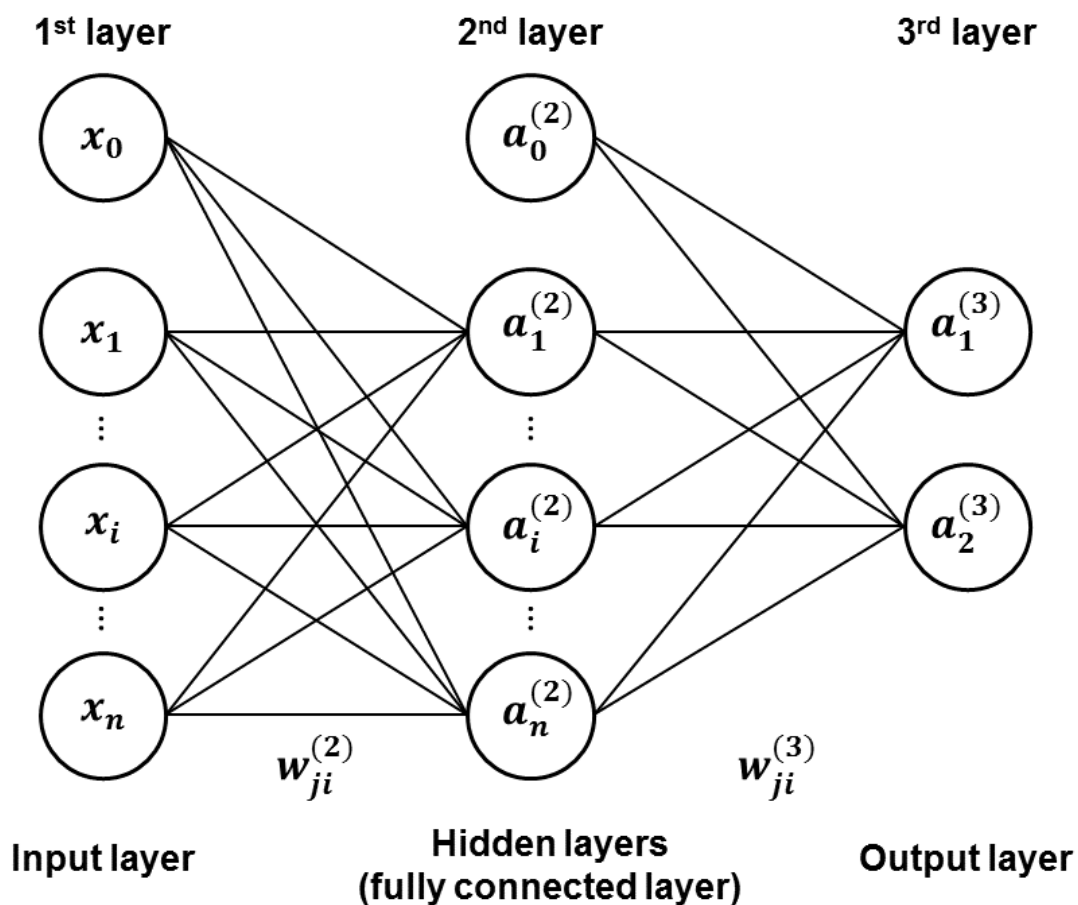
Figure 2.3. The structure of ANN consists of input layer, fully connected layer (hidden layer), and output layer.

fully connected layer, and output layer (see Fig. **2.4**).

For forward propagation in the training process, the convolutional filter in the convolutional layer is convolved with the input data. The convolutional filter usually has width size equal to dimensionality, d, of the input data and kernel size (height) of h, where the ith output from 1D convolution can be obtained by [56]

$$o_i = f(\mathbf{w} \cdot \mathbf{X}[i : i+h-1]) \tag{2.7}$$

and

$$m_i = f(o_i + b) \tag{2.8}$$

where $\mathbf{w}$ is the weight matrix of the convolutional filter with dimension of $h \times d$. The input matrix is defined as $\mathbf{X}$, where $\mathbf{X}[i : j]$ is the sub-matrix of the input from row i to j. o_i is the output, and m_i is the activation of o_i called feature map. Likewise ANN, the feature map from the current convolutional layer is the input data for the next convolutional layer.

After the convolutional layer, additional subsampling layer including max-pooling or dropout are added in order to enhance the performance of the neural net. Max-pooling [56] and dropout [57] are well-known methods to boost up performance in the deep learning. The max-pooling was used in order to reduce the size of data while keeping outstanding information. Dropout was introduced as a regularization technique for the deep learning to avoid
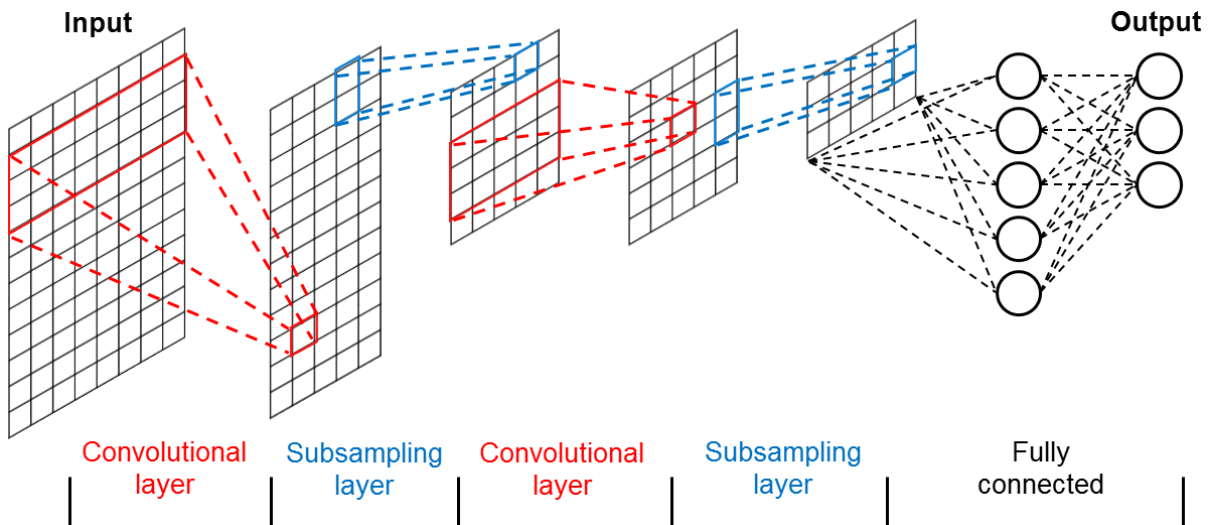
Figure 2.4. The structure of convolutional neural network consists of input, convolutional layer, subsampling layer, fully connected layer, and output.

overfitting by randomly dropping out one or more hidden nodes. The hyperparameters intro-
duced for ANN (i.e. learning rate, batch size, and number of epochs) should be also considered
in order to improve the performance of CNN.

4.   Evaluation

K-fold cross-validation is a statistical analysis that evaluates the performance of a predictive
model [52, 58]. Figure **2.5** represents the procedure of *k*-fold cross-validation. First, entire data
is divided equally into *k* folds. Then, every single fold is used as a test set and the remaining
folds are used as a training set. This process is repeated until each fold is used as a test set,
where the accuracy obtained from each of tested fold is averaged as described by

$$\bar{CV} = \frac{1}{K} \sum_{i=1}^{K} CV_i \tag{2.9}$$

where $\bar{CV}$ is the estimated performance of the predictive model, K is the total number of fold,
CV_i is the classification accuracy of the ith fold.
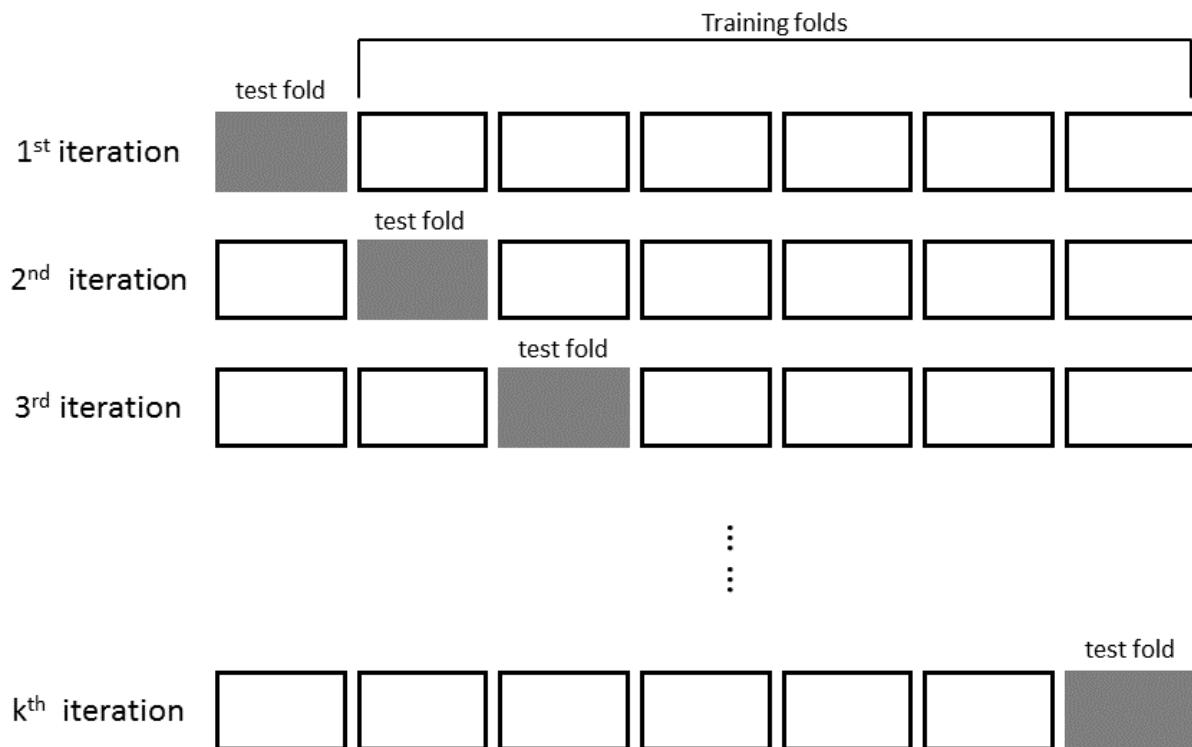
Figure 2.5. K-fold cross-validation procedure.

III. METHOD

1. Participants

A total of four healthy subjects were recruited in the experiment (all right-handed, mean age 23 ± 2.5, three females). Figure **3.1(a)** represents the subject during the signal measurement. None of the subjects has history of neurological disorder or surgery or brain injury. All the subjects were asked to avoid smoking and drinking alcohol or coffee within 3 hours prior to the experiment. A written consent forms were obtained from each participant. The experimental procedure was approved by the DGIST Institutional Review Board (DGIST-170414-HR-004-01).

2. Data Acquisition

The multichannel continuous wave fNIRS device, LABNIRS from Shimadzu, with three wavelengths (780, 805, and 830 nm) and sampling rate of 25.7 Hz was utilized to acquire hemodynamic response signal. A total of 34 channels combined from 12 pairs of light sources and detectors with distance 3 cm were placed over motor cortex area C3 and C4 based on international 10-20 system [59] which correspond to the motor area of right and left hand, respectively (see Fig. **3.1(b)**).

3. Experimental Procedure

In the experiment, subjects were asked to sit on a comfortable chair and relax to ensure that blood flow is steady. A monitor screen was placed in front of the subjects approximately 80 cm and displayed the tasks. Black screen, right arrow, and left arrow indicate rest, right hand finger tapping, and left hand finger tapping, respectively. Each subjects performed 10 experiments, each of which experiment is comprised of five repetitions of 10 seconds of rest, 10 seconds of right hand finger tapping, 10 seconds of rest, and 10 seconds of left hand finger tapping (see Fig. **3.2**). The experiment for all the subjects was conducted within three days. The total of

100 samples of rest, 50 samples of right and 50 samples of left hand motor executions were obtained from each subject.

4.   Preprocessing

4.1   Concentration Changes of Hemoglobin

The measured light intensities were converted into the concentration changes of HbO and HbR using MBLL. The MBLL equation is expressed by

$$
\begin{bmatrix} \Delta[HbO] \\ \Delta[HbR] \end{bmatrix} = \frac{1}{d \cdot DPF} \begin{bmatrix} \varepsilon_{\lambda 1}^{HbO} & \varepsilon_{\lambda 1}^{HbR} \\ \varepsilon_{\lambda 2}^{HbO} & \varepsilon_{\lambda 2}^{HbR} \end{bmatrix}^{-1} \begin{bmatrix} \Delta OD_{\lambda 1} \\ \Delta OD_{\lambda 2} \end{bmatrix} \tag{3.1}
$$

where the concentration changes of HbO and HbR are defined as $\Delta[HbO]$ and $\Delta[HbR]$, respectively. d is the distance between light source and detector set as 3 cm in the experiment. DPF is the differential path length factor. ε is the extinction coefficient at wavelength λ, and ΔOD is the optical density change.
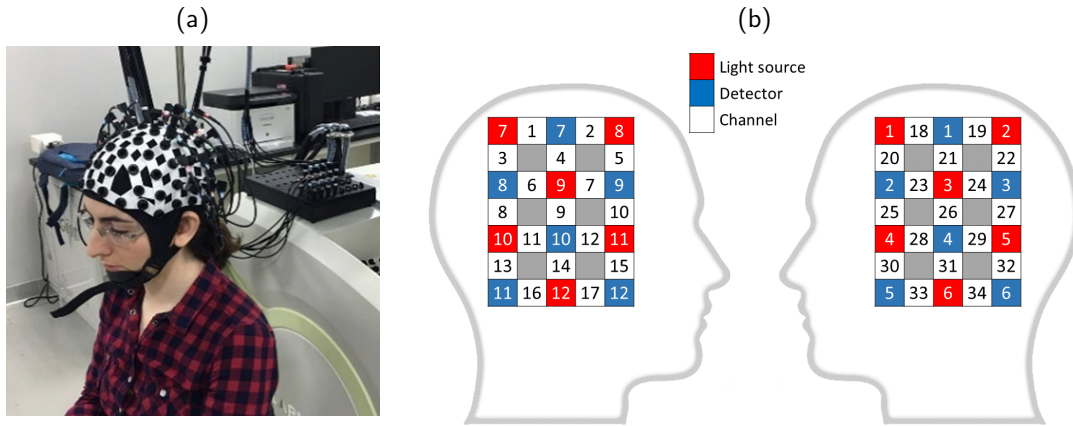
Figure 3.1. (a) A subject with optodes over right and left hemisphere. (b) The source and detector configuration in total of 34 channels. Channel number 1-17 and 18-34 were placed over motor area C4 and C3 based on the international 10-20 system, respectively.

Figure 3.2. Experimental procedure includes rest and two motor tasks: right and left hand motor execution. Each task lasts 10 seconds.

4.2 Filtering

The measured hemodynamic response signals contaminated by physiological noises including very low frequency oscillations, mayer wave, respiration, and heart rate at frequency of 0.03, 0.1, 0.2, and 0.8 Hz, respectively [37, 39, 43]. Figure **3.3** represents each component of physiological noises in hemodynamic response signal. In order to remove undesired physiological signal components, wavelet filtering was applied [60].

The wavelet transform is a method for time-frequency analysis which adjusts the window width in time and frequency domain. To remove undesired frequency components, wavelet transform expresses the signal, $S[n]$, by shifting and dilating wavelet mother function, and then remarkable coefficients related to hemodynamic response signal are reconstructed. For signal decomposition and reconstruction, multi-resolution analysis (MRA) based discrete wavelet transform (DWT) was exploited. By MRA based DWT, MRA decomposes the signal into tree structure using DWT, decomposed signals are an approximation coefficient (low-frequency component) and detailed coefficient (high-frequency component). The wavelet mother func-
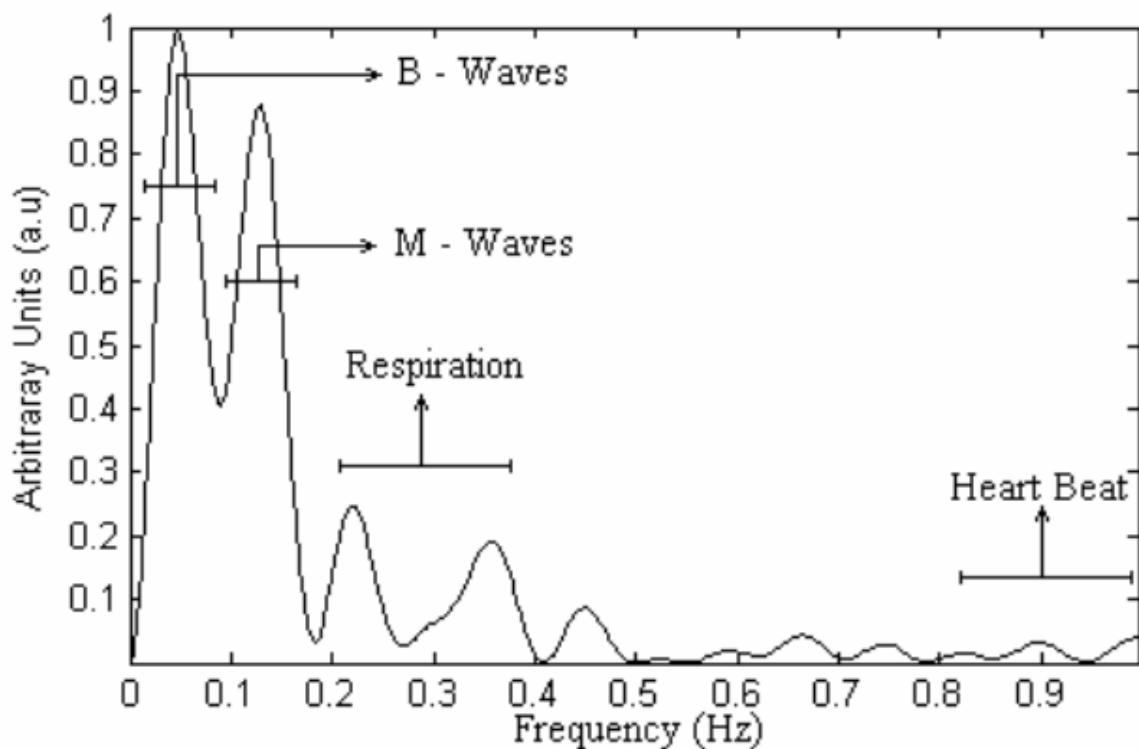
Figure 3.3. Physiological noises in fNIRS signal including heart rate, respiration, mayer wave (M-wave), and very low frequency oscillations (B-wave) (taken from [39]).

tion, approximation coefficients and detailed coefficients are computed by

$$\psi_{j,k}[n] = \frac{1}{\sqrt{j}}\psi(\frac{n-k}{j}), \tag{3.2}$$

$$A_\phi[j_0,k] = \frac{1}{\sqrt{M}}\sum_n S[n]\phi_{j_0,k}[n], \tag{3.3}$$

and

$$D_\psi[j,k] = \frac{1}{\sqrt{M}}\sum_n S[n]\psi_{j,k}[n], \tag{3.4}$$

where $\phi_{j_0,k}[n]$ is the scaling function, M is total points, $A_\phi[j_0,k]$ is approximation coefficients, $D_\psi[j,k]$ is detailed coefficients, and the wavelet mother function, $\psi_{j,k}$, is dilated with scaling parameter j which is greater than zero, and k is translating parameter. A signal S[n] is expressed by

$$S[n] = \frac{1}{\sqrt{M}}\sum_k A_\phi[j_0,k]\phi_{j_0,k}[n] + \frac{1}{\sqrt{M}}\sum_{j=j_0}^{\infty}\sum_k D_\psi[j,k]\psi_{j,k}[n]. \tag{3.5}$$

The approximation coefficients and detailed coefficients can be rewritten as

$$a_{j_0} = \frac{1}{\sqrt{M}}\sum_k A_\phi[j_0,k]\phi_{j_0,k}[n], \tag{3.6}$$

and

$$d_j = \frac{1}{\sqrt{M}}\sum_k D_\psi[j,k]\psi_{j,k}[n], \tag{3.7}$$

so, the signal $S[n]$ can be reconstructed from the detailed components by

$$S[n] = a_{j_0} + \sum_{j=-\infty}^{j_0} d_j. \tag{3.8}$$

The 10 level wavelet decomposition using Daubechies (db5) as wavelet mother function was applied in order to remove undesired high and low frequency components of physiological noises. The bandpass frequency between 0.02-0.1 Hz was desired to obtain the hemodynamic response signal. The combination of detailed components d_8 and d_9 from 10 level decompositions contains the signal corresponding to the frequency of 0.02-0.1 Hz, thus the filtered signal was reconstructed by $\tilde{S}[n] = d_8 + d_9$, where $\tilde{S}$ is filtered signal of the hemodynamic response

signal. After filtering, the hemodynamic response signals were rescaled into the range of [0,1].

5. Feature Extraction and Classification

After signal preprocessing, the conventional scheme of fNIRS-based BCI (SVM and ANN-based fNIRS) and the proposed scheme (CNN-based fNIRS) were trained and tested using hemodynamic response signals from each of the subject. The classification accuracies from the conventional methods and the proposed method were computed in the testing session. In this section, the details of the conventional scheme and proposed structure of CNN are described.

5.1 Conventional Method

In the conventional methods, the commonly used signal features of fNIRS-based BCI from the hemodynamic response were extracted manually (i.e. signal mean, peak, slope, variance, skewness, and kurtosis) [37]. The signal features were rescaled into a range of [0,1]. The input data consisted of 408 feature dimensions (6 features $\times$ 2 signals of HbO and HbR $\times$ 34 channels).

The SVM and ANN were used as classifiers since they have been reported as high performance classifiers in fNIRS-based BCI [37]. Before applying SVM, as such high-dimensional features usually suffer from performance degradation [61], thus principle component analysis (PCA) was applied in order to decrease the dimension of the data by maximizing variance with fewer number of principle components [51]. The regularization was likewise applied to reduce overfitting in ANN. The performances of the conventional methods (SVM and ANN-based) were estimated by computing classification accuracy using 10-fold cross-validation.

For further comprehensive investigation, different structures of ANN with different number of neurons in the hidden layers were considered. Table **3.1** represents the number of neurons and hidden layers in each structure of the ANN. All the hyperparameters were tuned for each individual subject (see Table **3.2**). In this thesis, the results of linear SVM and multiple structures of ANN were reported.

5.2 Proposed Structures of CNN

The CNN was employed as a classifier owing to its major property of performing feature extraction automatically. The signals of concentration changes of HbO and HbR were passed through convolutional layer of the CNN. Instead of extracting features from the hemodynamic response signals manually, the concentration changes of HbO and HbR were used as the input

Table 3.1. Number of neurons and hidden layers in the structure of the ANN.

Structure	Hidden layer	Neurons in each hidden layer
ANN-1a	1	128
ANN-1b	1	256
ANN-1c	1	512
ANN-2a	2	256 - 128
ANN-2b	2	512 - 256
ANN-2c	2	512 - 128

Table 3.2. Hyperparameter of each subject for training ANN.

Subject	Parameters	ANN-1a	ANN-1b	ANN-1c	ANN-2a	ANN-2b	ANN-2c
A	Epochs	100	100	50	50	50	100
	Batch size	32	32	32	64	16	64
	Learning rate	0.001	0.0005	0.0005	0.001	0.0005	0.001
B	Epochs	50	100	100	100	50	50
	Batch size	16	16	16	32	32	32
	Learning rate	0.001	0.0005	0.001	0.001	0.0005	0.001
C	Epochs	100	100	50	100	100	100
	Batch size	16	16	16	32	32	32
	Learning rate	0.001	0.001	0.0005	0.001	0.001	0.001
D	Epochs	50	50	100	100	50	50
	Batch size	64	64	64	32	64	16
	Learning rate	0.001	0.001	0.001	0.001	0.0005	0.0005

for the CNN. The input is M by N matrix where M is the number of data points during 10 seconds corresponding to the sampling rate ($M = time \times sampling\ rate \approx 257$) and N is the number of channels for both HbO and HbR (34 channels of each HbO and HbR).

Various numbers of convolutional layer and filters of the CNN structure were utilized for the comprehensive examination (see Table **3.3**). Each convolutional layer consists of convolutional filters with kernel size of 3, and the gradient descent algorithm was used to update weight value throughout learning process. All the convolutional filters in the convolutional layers performed 1D convolution with the input data along the vertical axis as shown in Fig. **3.4**.

The subsampling layers were applied after each convolutional layer to improve the CNN performance. As aforementioned, max-pooling and dropout have been introduced as techniques for improving the deep learning model, hence they were employed into the subsampling layer. Each subsampling layer contains max-pooling with kernel size of 2 followed by dropout with a dropout rate 50%.

The convolutional and subsampling layers were followed by two layers of the fully connected layers and the output layer. The first and second fully connected layers contain 256 and 128 neurons, and the output layer has 3 neurons corresponding to the three classes which were determined by using softmax. For better comprehension about the CNN structure, the convolutional and subsampling layers as well as input and output size of the proposed structure CNN-2a is clarified in Table **3.4**.

The activation function to transform the output also plays an important role in the deep

Table **3.3**. Number of convolutional layer and filters in each convolutional layer of the CNN.

Structure	Conv-layer	Filters in each Conv-layer	Neurons in each hidden layer
CNN-1a	1	16	256 - 128
CNN-1b	1	32	256 - 128
CNN-1c	1	64	256 - 128
CNN-2a	3	16 - 16 - 16	256 - 128
CNN-2b	3	32 - 32 - 32	256 - 128
CNN-2c	3	64 - 64 - 64	256 - 128

learning. In the proposed structure, all activation functions were set to the rectified linear unit (ReLU) which is non-linear function. In comparison with other activation functions, ReLU has major benefit of converging to the optimum point much faster in practice and avoiding vanishing gradient which inhibits the update of weight values in the deep layers. Consequently, ReLU was implemented as an activation function to enhance the performance in the training process of deep neural network on large scale and complex datasets. The function of ReLU can

Table 3.4. Input and output size of the proposed structure CNN-2a

Layer	Input Size	Output Size	Properties
Convolutional layer 1	257, 68	257, 16	16 filters with kernel size 3
Max-pooling 1	257, 16	128, 16	kernel size 2
Dropout 1	128, 16	128, 16	dropout rate 50%
Convolutional layer 2	128, 16	128, 16	16 filters with kernel size 3
Max-pooling 2	128, 16	64, 16	kernel size 2
Dropout 2	64, 16	64, 16	dropout rate 50%
Convolutional layer 3	64, 16	64, 16	16 filters with kernel size 3
Max-pooling 3	64, 16	32, 16	kernel size 2
Dropout 3	32, 16	32, 16	dropout rate 50%
Fully connected layer 1	512	256	256 hidden nodes
Fully connected layer 2	256	128	128 hidden nodes
Output layer	128	3	3 hidden nodes
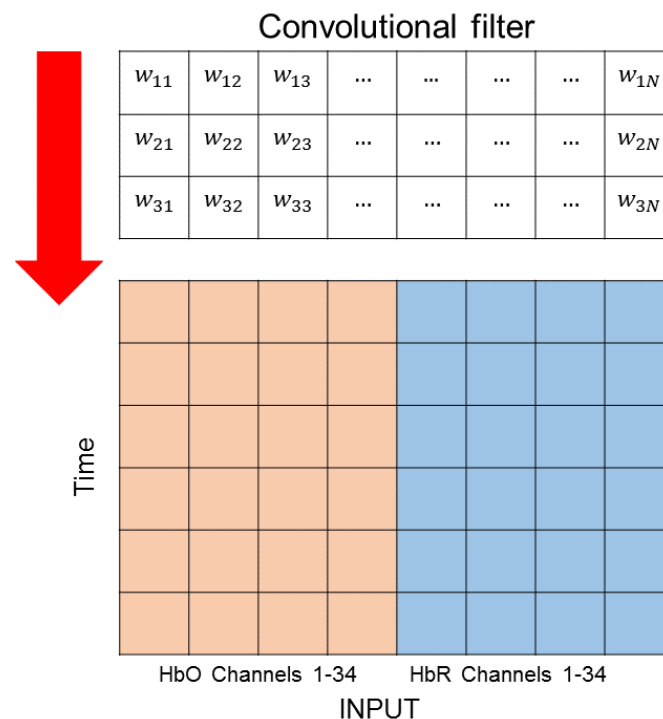
Figure 3.4. The input data consisted of the concentration changes of HbO (red) and HbR (blue) overall channels. A convolutional filter move through the input data along the vertical axis.

be expressed by [62]

$$a(x) = \begin{cases} 0 & \text{if } o_i < 0 \\ \\ o_i & \text{if } o_i \geq 0. \end{cases} \tag{3.9}$$

Additionally, Table **3.5** represents the hyperparameters for training the CNN of each individual subject including epochs, batch size, and learning rate determined by using grid search [52, 63] and 10-fold cross-validation. The Adam was utilized as a gradient descent optimization algorithms, where its parameters β_1, β_2, and ε were set to 0.9, 0.1, and 10^{-8}, respectively [64].

Table 3.5. Hyperparameter of each subject for training CNN.

Subject	Parameters	CNN-1a	CNN-1b	CNN-1c	CNN-2a	CNN-2b	CNN-2c
A	Epochs	100	100	100	50	100	100
	Batch size	16	64	16	16	16	32
	Learning rate	0.0005	0.001	0.0005	0.0005	0.001	0.001
B	Epochs	50	50	50	100	100	100
	Batch size	32	16	64	16	64	16
	Learning rate	0.001	0.001	0.001	0.0005	0.001	0.0005
C	Epochs	100	50	50	100	100	100
	Batch size	16	16	32	64	32	32
	Learning rate	0.0001	0.0001	0.0005	0.0005	0.0001	0.001
D	Epochs	100	50	100	100	50	50
	Batch size	16	16	16	64	64	32
	Learning rate	0.0005	0.001	0.0005	0.0005	0.0005	0.001

6. Feature Visualization

In this thesis, the CNN was proposed as a method to improve the classification accuracy in fNIRS-based BCI due to the automatic feature extraction. To interpret the feature extraction

performance, the visualization of the hemodynamic response signal, commonly used features, and feature map of the CNN were compared. Figure **3.5** represents the overall procedure to visualize the aforementioned features. As high-dimensional data is complicated to visualize, the PCA was employed to reduce the dimensionality. The first and second principle components from PCA were extracted for the visualization.

To estimate the distribution between each class, the first and second components of the PCA were rescaled into [0,1] and used as the input data. The global and local mean of each class are computed as

$$\boldsymbol{\mu}^g = \frac{1}{N} \sum_{i=1}^{N} p_i \tag{3.10}$$

and

$$\boldsymbol{\mu}^j = \frac{1}{n^j} \sum_{i=1}^{n^j} p_i^j \tag{3.11}$$

where $\boldsymbol{\mu}^g$ is the global mean, $\boldsymbol{\mu}^j$ is the local mean of class j, p_i is the data point at i^{th}, p_i^j is the data point at i^{th} of class j, and n^j is the number of samples of class j. The euclidean distance between $\mathbf{q_1}$ and $\mathbf{q_2}$ is obtained by

$$d(\mathbf{q_1}, \mathbf{q_2}) = \sqrt{\sum_{i=1}^{m} (q_{1,i} - q_{2,i})^2} \tag{3.12}$$

where $d(\mathbf{q_1}, \mathbf{q_2})$ is the euclidean distance between $\mathbf{q_1}$ and $\mathbf{q_2}$, and m is the space of $\mathbf{q_1}$ and $\mathbf{q_2}$. The estimation of the distribution between each class is obtained from

$$R^j = \frac{d(\boldsymbol{\mu}^j, \boldsymbol{\mu}^g)}{E(d(\mathbf{P}^j, \boldsymbol{\mu}^j))} \tag{3.13}$$

where E($\mathbf{X}$) is the expected value of matrix $\mathbf{X}$, $\mathbf{P}^j$ is a matrix of data point in class j, and R^j is the ratio of the euclidean distance between $\boldsymbol{\mu}^g$ and $\boldsymbol{\mu}^j$ to the expected value of euclidean distances between $\mathbf{P}^j$ and $\boldsymbol{\mu}^j$ of class j. In the case that all the classes are well separated, R^j value is expected to be large.
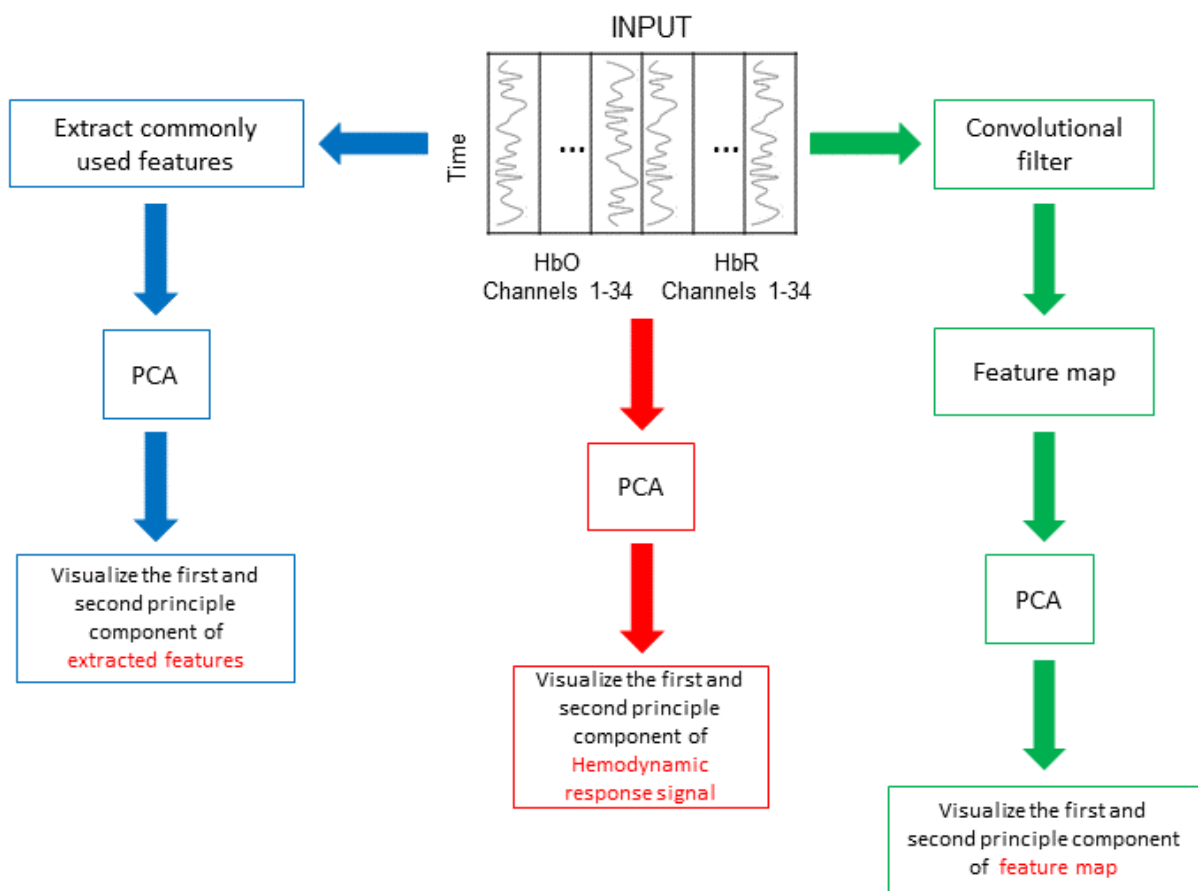
Figure 3.5. The overall procedure to visualize hemodynamic response signal, commonly used features, and feature map by extracting the first two principle components from PCA.

IV.   RESULTS AND DISCUSSIONS

1.   Measured Hemodynamic Responses

In the experiment, the concentration changes of HbO and HbR were measured from each subject and used as the input data to train the CNN, and signal features extracted from the measured signal were used to train ANN and SVM. The hemodynamic response signals across full sessions of each task: rest, right and left hand motor executions, were averaged as shown in Fig. **4.1(a)**, **4.1(b)**, and **4.1(c)**, respectively. The vertical and horizontal axis of the input data indicate each channel and the hemodynamic response signal while performing tasks, respectively. The signal amplitude is represented by the color intensities of red and blue which imply maximum and minimum amplitude, respectively. From beginning to end of the tasks correspond to 0 to 10 seconds.

It has been reported that the changes of the cerebral blood oxygenation induced by neural activity lead to the increment of HbO and decrement of HbR concentration changes in the local area [38]. In the measured hemodynamic response, similar behavior of the hemodynamic response could be observed as shown in Fig. **4.1**. The hemodynamic response signal obtained over C3 indicted relatively higher cortical activation during 5-10 seconds in the right hand motor execution as shown in Fig. **4.1(b)**. While, the hemodynamic response signal over C4 showed higher activation in the left hand motor execution as shown in Fig. **4.1(c)**.

Figure **4.2** represents the averaged signal across the sessions overall channels of both left and right hemispheres. As the experimental protocol was the repetition of rest followed by task, the HbO responses decreased with time (see Fig.**4.2(a)**). The concentration changes of HbO was obviously higher than HbR in the left hemisphere during right hand motor execution as shown in Fig. **4.2(b)**. Unlike, the concentration change of HbO was higher in the right hemisphere during the left hand motor execution as shown in Fig. **4.2(c)**. Figure **4.2(b)** and **(c)** also show the increment of HbO over the other hemisphere or non-corresponding area, since a reduction in local oxygen caused by neural activity increases the CBF, and arteriolar vasodilation responses to increase the local CBF. However, the hemodynamic response measured from

the experiment indicates the possibility of discriminating three-class: rest, right and left hand motor executions, since the brain response showed the differences of cortical activation over the left and right hemispheres.

2. Classification Accuracy

The hemodynamic response signal of three-class: rest, left, and right hand motor executions, were discriminated by the conventional scheme (SVM and ANN-based fNIRS) and the proposed scheme (CNN-based fNIRS). The classification accuracies of both schemes were calculated by 10-fold cross-validation in order to estimate the performance. Table **4.1** represents
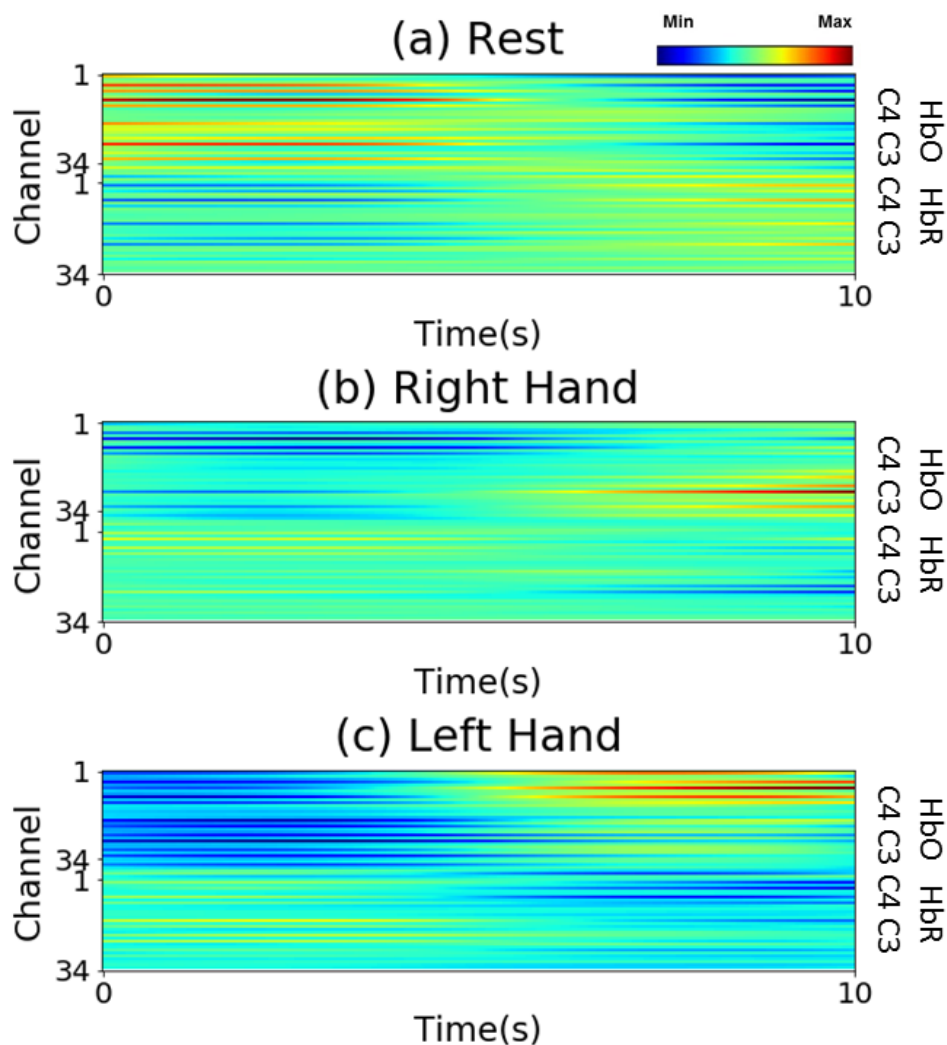
Figure 4.1. Average result of each execution measured from subject-B: (a) rest, (b) right and (c) left hand motor execution. Each input presents concentration changes of HbO and HbR overall 34 channels. Red and blue colors represent maximum and minimum amplitude, respectively.
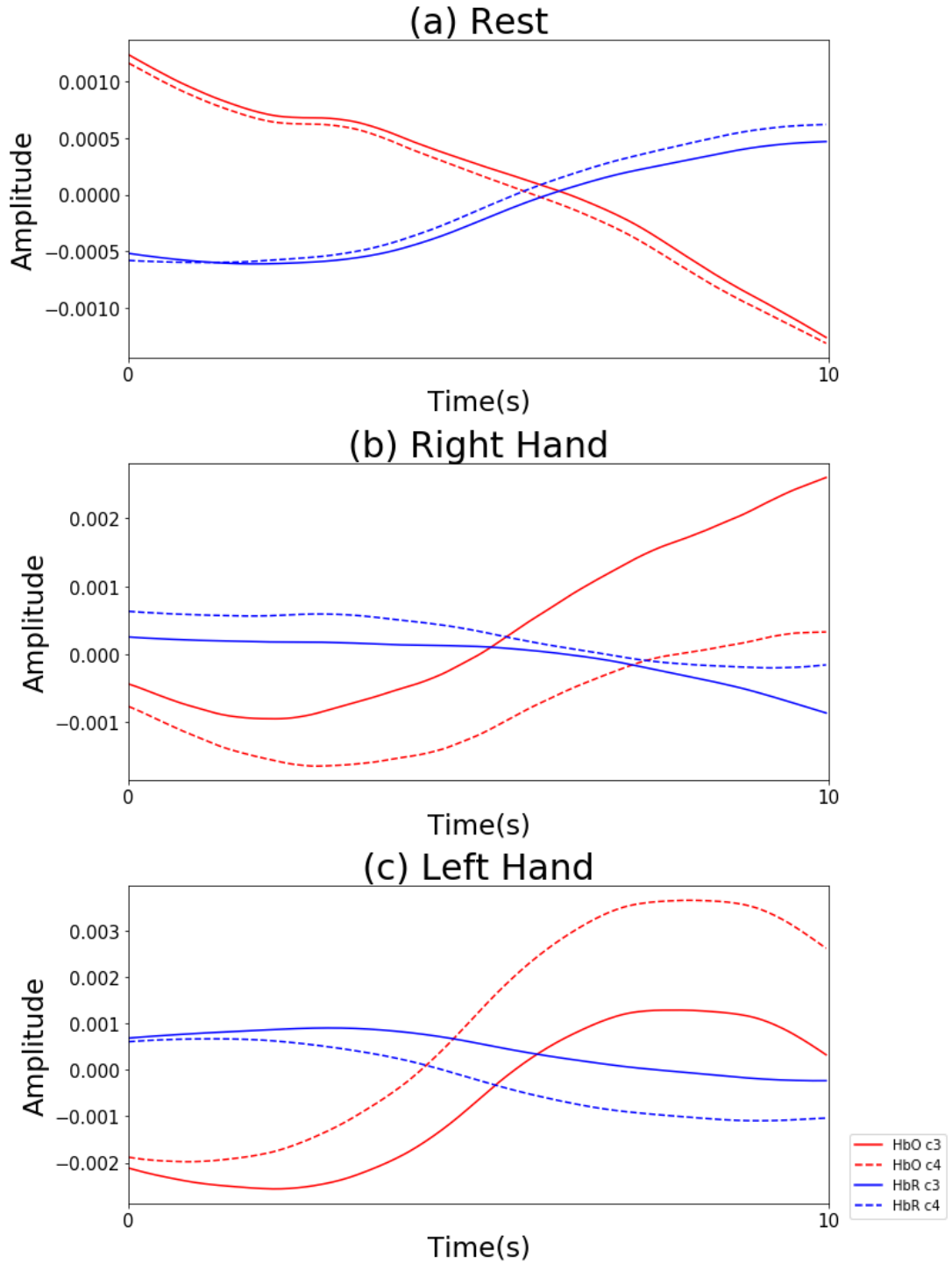
Figure 4.2. Average signal amplitude of subject-B across all sessions of left (C3) and right (C4) hemisphere of each class: (a) rest, (b) right and (c) left hand motor execution. Red and blue colors imply the concentration changes of HbO and HbR, respectively. Solid and dot lines are related to the C3 and C4 motor areas in that order

the classification accuracies of subject-A, -B, -C, and -D from both conventional and proposed schemes. Since various structures of ANN and CNN were examined, the structure ANN-2b and CNN-1b which achieved the highest classification accuracy were selected for the com-

parison. The classification accuracies of SVM, ANN (ANN-2b), and CNN (CNN-1b) from each individual subject is shown in Fig. **4.3**. It shows that the classification accuracy of CNN outperforms both SVM and ANN in three out of four subjects. In the statistical assessment, the average accuracies across all the subjects of SVM, ANN, and CNN (84.00%, 87.17%, and 90.92%, respectively) indicate the superior performance of CNN over the conventional methods. The CNN shows the excellent performance in consequence of its capability of learning the patterns from the input data by optimizing the weight values through the training process.

3. Feature Visualization

The CNN is able to learn and recognize the patterns of three-class: rest, right and left hand motor executions, based on updating the weight values of the filters in the convolutional layer and hidden layer. In this section, the structure CNN-1b of the CNN was investigated that the CNN transforms the input data into better separable feature by convolving the input with convolutional filter.

While convolutional methods perform feature extraction manually, CNN is remarkable to extract proper features automatically. To better understand the feature extraction performance, the hemodynamic response signal and feature extracted by conventional methods and convolutional filter were visualized by plotting the first two principle components of PCA. Figure

Table 4.1. Classification accuracies of each subject (%)

Structure	Subject-A	Subject-B	Subject-C	Subject-D	Average
SVM	88.50	79.00	84.00	84.50	84.00
ANN-1a	91.50	79.00	85.00	83.17	84.67
ANN-1b	92.67	81.00	84.83	85.00	85.86
ANN-1c	91.83	83.33	84.83	85.33	86.33
ANN-2a	91.33	82.50	85.16	85.67	86.16
ANN-2b	91.67	84.00	85.33	87.67	87.17
ANN-2c	92.17	82.67	85.50	86.17	86.63
CNN-1a	92.17	90.00	85.00	93.33	90.12
CNN-1b	92.67	90.83	85.00	95.17	90.92
CNN-1c	92.17	89.50	84.83	94.33	90.21
CNN-2a	92.50	90.33	82.33	91.33	89.12
CNN-2b	92.67	91.33	81.50	92.83	89.59
CNN-2c	92.50	90.17	83.00	92.17	89.46

4.4 illustrate the visualizations of the above-mentioned features from subject-A and subject-B which explicitly shows the outputs from the convolutional filter was better discriminating compared with the others.

When considering just the binary classification of rest and motor execution, both the conventional methods and CNN resulted in the well separable features. However, for the multi-class or binary classification of right and left motor executions, CNN was be able to extract better discriminated features as compared with the conventional methods.

Table **4.2** represents the values of the ratio obtained from Eq. 3.13. The higher ratio implies that the data were well discriminated between all the classes, while lower ratio indicates poor separable data. The average ratio values across all the subjects of the feature map, hemodynamic response, and commonly used features (1.22, 0.68, and 0.66, respectively) confirmed that the features extracted by convolutional filter were better discriminated compared with the others.

Consequently, the proposed method will be appropriate for various applications that require multi tasks to command or vital applications. For instance, a brain-controlled wheelchair for a patient with severe motor impairment require high accuracy and multi tasks to control
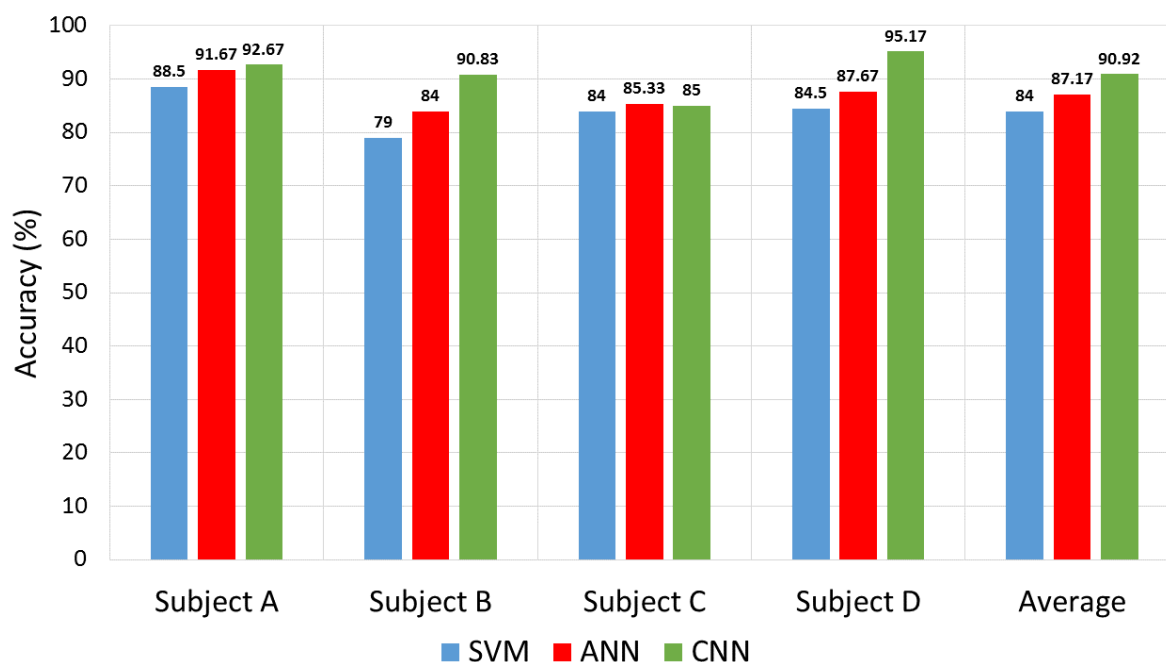
Figure 4.3. Average classification accuracies of each method. The classification accuracies of SVM, ANN, and CNN are represented in blue, red, and green bar.

wheelchair in several directions, since any misclassification would probably lead to a serious accident.

4.   Future Work

While many studies have investigated on the various feature combinations and machine learning algorithms to achieve high classification accuracy in fNIRS-based BCI, the proposed CNN as feature extractor and classifier demonstrated the gain in performance over conventional scheme. However, only classical machine learning algorithm (SVM) and classifier reported as the most appropriate in fNIRS-based BCI (ANN) [50] with commonly used features in time-domain signal (signal mean, peak, slope, variance, skewness, and kurtosis) were used as conventional schemes. Other features and machine learning algorithms needed to be investigated for more comprehensive study.

In this thesis, the CNN was proposed as a promising method to discriminate hemodynamic
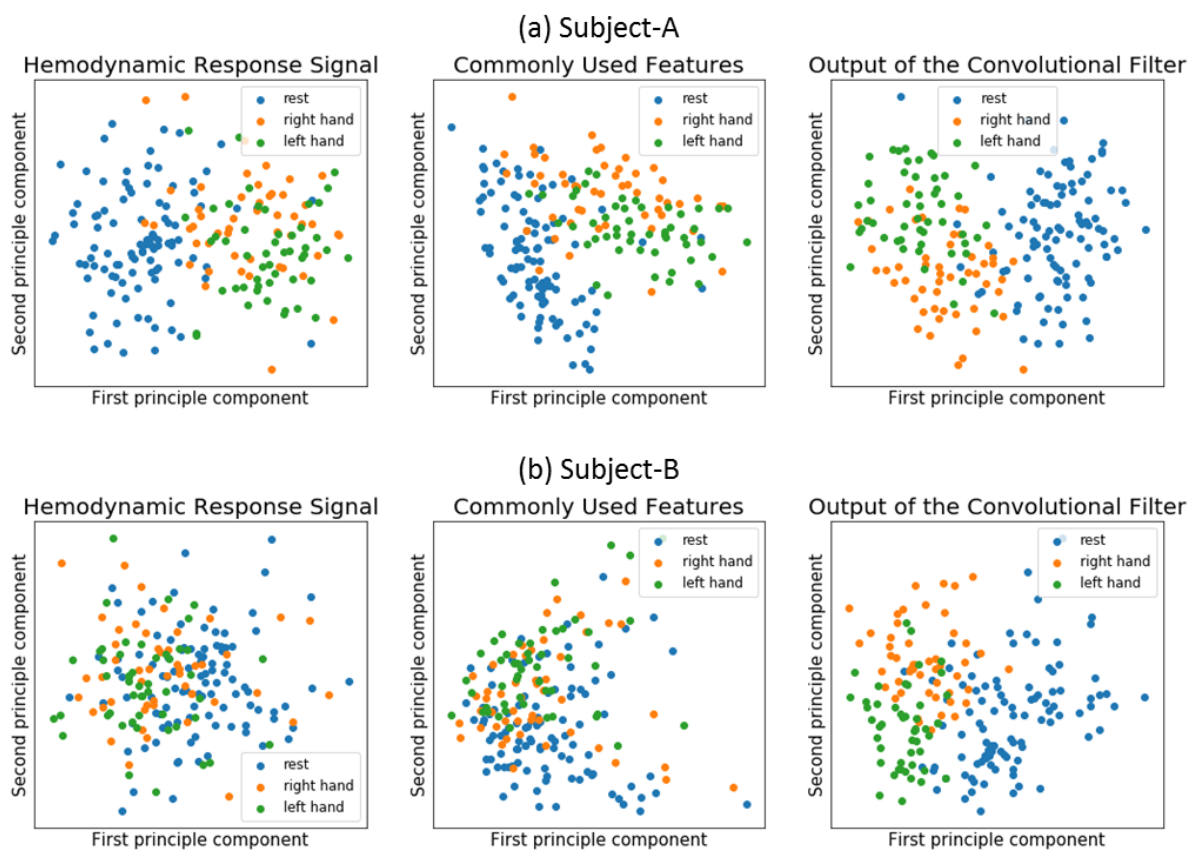
Figure 4.4. The visualization of the signal including hemodynamic response signal, commonly used features, and output of the convolutional filter (feature map) from subject-A and subject-B.

Table 4.2. The ratio of the distance between global and local mean to the average distance between each data point and local mean.

Subject	Input	Rest	Right Hand	Left Hand	Average
A	**Feature Map**	1.03	1.19	1.58	1.27
	Hemodynamic Response	0.92	0.81	1.25	1.00
	Commonly used features	0.78	0.80	1.12	0.90
B	**Feature Map**	0.76	1.31	1.47	1.18
	Hemodynamic Response	0.32	0.22	0.53	0.36
	Commonly used features	0.41	0.16	0.70	0.42
C	**Feature Map**	0.87	0.92	0.88	0.89
	Hemodynamic Response	0.92	0.97	0.93	0.94
	Commonly used features	0.84	1.01	1.00	0.95
D	**Feature Map**	0.78	1.93	1.86	1.52
	Hemodynamic Response	0.44	0.47	0.42	0.44
	Commonly used features	0.41	0.39	0.32	0.38

response signal in fNIRS-based BCI. The results implied that the use of CNN yields better performance in terms of classification accuracy over conventional schemes. As the classification accuracy plays the most important role in BCI, future work will implement various techniques in deep learning for further improvement of the accuracy.

The experiment was conducted merely with healthy subjects. However, the cortical activation in the patients with brain injury or motor disabilities probably be dissimilar to healthy people. Accordingly, the future work will explore the study to examine the feasibility of using fNIRS-based BCI in the patients with motor impairment. Additionally, the experimental protocol was designed for the initial study. To imitate the use in real application, the experimental protocol will be improved in the future study.

This thesis examined the use of CNN in fNIRS-based BCI with offline signal processing and classification. However, the final goal of BCI is to operate the system in real-time, thus the future study will include the investigation of online signal processing as well as signal classification for fNIRS-based BCI.

V. CONCLUSION

In the last few decades, BCI researches have implemented fNIRS for measuring brain signal, since it offers many benefits over other modalities. To enhance the classification accuracy for BCI system, the conventional scheme of fNIRS-based BCI primarily focused on finding the appropriate feature such as signal mean, peak, slope, variance, kurtosis, and skewness, and the machine learning algorithm such as SVM and ANN.

The main objective of this thesis is to improve the classification accuracy of fNIRS-based BCI by classifying and extracting feature automatically. To this end, the proposed method using CNN was compared with the conventional methods using SVM and ANN. Related to the first research question, the results indicated that the CNN-based method outperforms both SVM and ANN-based methods with the gain in accuracy up to 6.92% and 3.75%, respectively. Additionally, the features extracted by the convolutional filter of CNN were better discriminating, as illustrated in the visualization, compared with the conventional methods which answers the second research question.

In summary, the results demonstrates the feasibility of using CNN as feature extractor and classification method for fNIRS-based BCI, since it shows the performance over conventional scheme as well as its capability of learning and generalizing feature from the input automatically.

References

[1] J. J. Daly and J. R. Wolpaw, "Brain–computer interfaces in neurological rehabilitation," *The Lancet Neurology*, vol. 7, no. 11, pp. 1032–1043, 2008.

[2] T. O. Zander and C. Kothe, "Towards passive brain–computer interfaces: applying brain–computer interface technology to human–machine systems in general," *Journal of Neural Engineering*, vol. 8, no. 2, p. 025005, 2011.

[3] J. R. Wolpaw, N. Birbaumer, W. J. Heetderks, D. J. McFarland, P. H. Peckham, G. Schalk, E. Donchin, L. A. Quatrano, C. J. Robinson, T. M. Vaughan, *et al.*, "Brain-computer interface technology: a review of the first international meeting," *IEEE Transactions on Rehabilitation Engineering*, vol. 8, no. 2, pp. 164–173, 2000.

[4] J. R. Wolpaw, N. Birbaumer, D. J. McFarland, G. Pfurtscheller, and T. M. Vaughan, "Brain–computer interfaces for communication and control," *Clinical Neurophysiology*, vol. 113, no. 6, pp. 767–791, 2002.

[5] G. Dornhege, *Toward brain-computer interfacing*. MIT Press, 2007.

[6] R. P. Rao, *Brain-computer interfacing: an introduction*. Cambridge University Press, 2013.

[7] C. Neuper, G. R. Müller-Putz, R. Scherer, and G. Pfurtscheller, "Motor imagery and EEG-based control of spelling devices and neuroprostheses," *Progress in Brain Research*, vol. 159, pp. 393–409, 2006.

[8] K. LaFleur, K. Cassady, A. Doud, K. Shades, E. Rogin, and B. He, "Quadcopter control in three-dimensional space using a noninvasive motor imagery-based brain–computer interface," *Journal of Neural Engineering*, vol. 10, no. 4, p. 046003, 2013.

[9] E. Buch, C. Weber, L. G. Cohen, C. Braun, M. A. Dimyan, T. Ard, J. Mellinger, A. Caria, S. Soekadar, A. Fourkas, *et al.*, "Think to move: a neuromagnetic brain-computer interface (BCI) system for chronic stroke," *Stroke*, vol. 39, no. 3, pp. 910–917, 2008.

[10] K. Saita, T. Morishita, K. Hyakutake, H. Fukuda, E. Shiota, Y. Sankai, and T. Inoue, "Combined therapy using botulinum toxin a and single-joint hybrid assistive limb for upper-limb disability due to spastic hemiplegia," *Journal of the Neurological Sciences*, vol. 373, pp. 182–187, 2017.

[11] U. Chaudhary, B. Xia, S. Silvoni, L. G. Cohen, and N. Birbaumer, "Brain–computer interface–based communication in the completely locked-in state," *PLoS Biology*, vol. 15, no. 1, p. e1002593, 2017.

[12] U. Chaudhary, N. Birbaumer, and M. Curado, "Brain-machine interface (BMI) in paralysis," *Annals of Physical and Rehabilitation Medicine*, vol. 58, no. 1, pp. 9–13, 2015.

[13] G. Pfurtscheller, G. R. Müller-Putz, J. Pfurtscheller, and R. Rupp, "EEG-based asynchronous BCI controls functional electrical stimulation in a tetraplegic patient," *EURASIP Journal on Applied Signal Processing*, vol. 2005, pp. 3152–3155, 2005.

[14] K. L. Koenraadt, J. Duysens, H. Rijken, I. J. van Nes, and N. L. Keijsers, "Preserved foot motor cortex in patients with complete spinal cord injury: A functional near-infrared spectroscopic study," *Neurorehabilitation and Neural Repair*, vol. 28, no. 2, pp. 179–187, 2014.

[15] S. Fazli, J. Mehnert, J. Steinbrink, G. Curio, A. Villringer, K.-R. Müller, and B. Blankertz, "Enhanced performance by a hybrid NIRS–EEG brain computer interface," *Neuroimage*, vol. 59, no. 1, pp. 519–529, 2012.

[16] N. Birbaumer, N. Ghanayim, T. Hinterberger, I. Iversen, B. Kotchoubey, A. Kübler, J. Perelmouter, E. Taub, and H. Flor, "A spelling device for the paralysed," *Nature*, vol. 398, no. 6725, pp. 297–298, 1999.

[17] M. Cheng, X. Gao, S. Gao, and D. Xu, "Design and implementation of a brain-computer interface with high transfer rates," *IEEE Transactions on Biomedical Engineering*, vol. 49, no. 10, pp. 1181–1186, 2002.

[18] A. Buttfield, P. W. Ferrez, and J. R. Millan, "Towards a robust BCI: error potentials and online learning," *IEEE Transactions on Neural Systems and Rehabilitation Engineering*, vol. 14, no. 2, pp. 164–168, 2006.

[19] B. Blankertz, G. Dornhege, M. Krauledat, K.-R. Müller, and G. Curio, "The non-invasive berlin brain–computer interface: fast acquisition of effective performance in untrained subjects," *Neuroimage*, vol. 37, no. 2, pp. 539–550, 2007.

[20] J. Mellinger, G. Schalk, C. Braun, H. Preissl, W. Rosenstiel, N. Birbaumer, and A. Kübler, "An MEG-based brain–computer interface (BCI)," *Neuroimage*, vol. 36, no. 3, pp. 581–593, 2007.

[21] E. C. Leuthardt, G. Schalk, J. R. Wolpaw, J. G. Ojemann, and D. W. Moran, "A brain–computer interface using electrocorticographic signals in humans," *Journal of Neural Engineering*, vol. 1, no. 2, p. 63, 2004.

[22] T. N. Lal, T. Hinterberger, G. Widman, M. Schröder, N. J. Hill, W. Rosenstiel, C. E. Elger, B. Schölkopf, and N. Birbaumer, "Methods towards invasive human brain computer interfaces.," *NIPS*, vol. 737–744, 2004.

[23] S. M. LaConte, "Decoding fMRI brain states in real-time," *Neuroimage*, vol. 56, no. 2, pp. 440–454, 2011.

[24] N. Weiskopf, K. Mathiak, S. W. Bock, F. Scharnowski, R. Veit, W. Grodd, R. Goebel, and N. Birbaumer, "Principles of a brain-computer interface (BCI) based on real-time functional magnetic resonance imaging (fMRI)," *IEEE Transactions on Biomedical Engineering*, vol. 51, no. 6, pp. 966–970, 2004.

[25] B. Sorger, B. Dahmen, J. Reithler, O. Gosseries, A. Maudoux, S. Laureys, and R. Goebel, "Another kind of BOLD Response: answering multiple-choice questions via online decoded single-trial brain signals," *Progress in Brain Research*, vol. 177, pp. 275–292, 2009.

[26] N. Naseer and K.-S. Hong, "Classification of functional near-infrared spectroscopy signals corresponding to the right-and left-wrist motor imagery for development of a brain–computer interface," *Neuroscience Letters*, vol. 553, pp. 84–89, 2013.

[27] K.-S. Hong, N. Naseer, and Y.-H. Kim, "Classification of prefrontal and motor cortex signals for three-class fNIRS–BCI," *Neuroscience Letters*, vol. 587, pp. 87–92, 2015.

[28] M. J. Khan, M. J. Hong, and K.-S. Hong, "Decoding of four movement directions using hybrid NIRS-EEG brain-computer interface," *Frontiers in Human Neuroscience*, vol. 8, p. 244, 2014.

[29] R. Sitaram, H. Zhang, C. Guan, M. Thulasidas, Y. Hoshi, A. Ishikawa, K. Shimizu, and N. Birbaumer, "Temporal classification of multichannel near-infrared spectroscopy signals of motor imagery for developing a brain–computer interface," *Neuroimage*, vol. 34, no. 4, pp. 1416–1427, 2007.

[30] J. Shin and J. Jeong, "Multiclass classification of hemodynamic responses for performance improvement of functional near-infrared spectroscopy-based brain–computer interface," *Journal of Biomedical Optics*, vol. 19, no. 6, pp. 067009–067009, 2014.

[31] S. M. Coyle, T. E. Ward, and C. M. Markham, "Brain–computer interface using a simplified functional near-infrared spectroscopy system," *Journal of Neural Engineering*, vol. 4, no. 3, p. 219, 2007.

[32] Y. Bengio, Y. LeCun, *et al.*, "Scaling learning algorithms towards AI," *Large-Scale Kernel Machines*, vol. 34, no. 5, pp. 1–41, 2007.

[33] P. Y. Simard, D. Steinkraus, J. C. Platt, *et al.*, "Best practices for convolutional neural networks applied to visual document analysis.," in *ICDAR*, vol. 3, pp. 958–962, Citeseer, 2003.

[34] D. Silver, A. Huang, C. J. Maddison, A. Guez, L. Sifre, G. Van Den Driessche, J. Schrittwieser, I. Antonoglou, V. Panneershelvam, M. Lanctot, *et al.*, "Mastering the game of go with deep neural networks and tree search," *Nature*, vol. 529, no. 7587, pp. 484–489, 2016.

[35] Y. Bengio *et al.*, "Learning deep architectures for AI," *Foundations and Trends in Machine Learning*, vol. 2, no. 1, pp. 1–127, 2009.

[36] S. Sukittanon, A. C. Surendran, J. C. Platt, and C. J. Burges, "Convolutional networks for speech detection.," in *Interspeech*, Citeseer, 2004.

[37] N. Naseer and K.-S. Hong, "fNIRS-based brain-computer interfaces: a review," *Frontiers in Human Neuroscience*, vol. 9, p. 3, 2015.

[38] F. Scholkmann, S. Kleiser, A. J. Metz, R. Zimmermann, J. M. Pavia, U. Wolf, and M. Wolf, "A review on continuous wave functional near-infrared spectroscopy and imaging instrumentation and methodology," *Neuroimage*, vol. 85, pp. 6–27, 2014.

[39] H. Liang, J. D. Bronzino, and D. R. Peterson, *Biosignal Processing: Principles and Practices*. CRC Press, 2012.

[40] F. Matthews, B. A. Pearlmutter, T. E. Wards, C. Soraghan, and C. Markham, "Hemodynamics for brain-computer interfaces," *IEEE Signal Processing Magazine*, vol. 25, no. 1, pp. 87–94, 2008.

[41] H.-J. Hwang, J.-H. Lim, D.-W. Kim, and C.-H. Im, "Evaluation of various mental task combinations for near-infrared spectroscopy-based brain-computer interfaces," *Journal of Biomedical Optics*, vol. 19, no. 7, pp. 077005–077005, 2014.

[42] X. Cui, S. Bray, and A. L. Reiss, "Functional near infrared spectroscopy (NIRS) signal improvement based on negative correlation between oxygenated and deoxygenated hemoglobin dynamics," *Neuroimage*, vol. 49, no. 4, pp. 3039–3046, 2010.

[43] S. Weyand, L. Schudlo, K. Takehara-Nishiuchi, and T. Chau, "Usability and performance-informed selection of personalized mental tasks for an online near-infrared spectroscopy brain-computer interface," *Neurophotonics*, vol. 2, no. 2, pp. 025001–025001, 2015.

[44] D. P.-O. Bos, M. Poel, and A. Nijholt, "A study in user-centered design and evaluation of mental tasks for BCI," in *International Conference on Multimedia Modeling*, pp. 122–134, Springer, 2011.

[45] B. Abibullaev and J. An, "Classification of frontal cortex haemodynamic responses during cognitive tasks using wavelet transforms and machine learning algorithms," *Medical Engineering & Physics*, vol. 34, no. 10, pp. 1394–1410, 2012.

[46] T. Q. D. Khoa and M. Nakagawa, "Functional near infrared spectroscope for cognition brain tasks by wavelets analysis and neural networks," *International Journal of Biological and Medical Sciences*, vol. 1, no. 28–33, 2008.

[47] V. Kaiser, G. Bauernfeind, A. Kreilinger, T. Kaufmann, A. Kübler, C. Neuper, and G. R. Müller-Putz, "Cortical effects of user training in a motor imagery based brain–computer interface measured by fNIRS and EEG," *Neuroimage*, vol. 85, pp. 432–444, 2014.

[48] X. Cui, S. Bray, and A. L. Reiss, "Speeded near infrared spectroscopy (NIRS) response detection," *PLoS One*, vol. 5, no. 11, p. e15474, 2010.

[49] B. Abibullaev, J. An, and J.-I. Moon, "Neural network classification of brain hemodynamic responses from four mental tasks," *International Journal of Optomechatronics*, vol. 5, no. 4, pp. 340–359, 2011.

[50] N. Naseer, N. K. Qureshi, F. M. Noori, and K.-S. Hong, "Analysis of different classification techniques for two-class functional near-infrared spectroscopy-based brain-computer interface," *Computational Intelligence and Neuroscience*, vol. 2016, 2016.

[51] J. L. Semmlow and B. Griffel, *Biosignal and medical image processing*. CRC Press, 2014.

[52] C.-W. Hsu, C.-C. Chang, C.-J. Lin, *et al.*, "A practical guide to support vector classification," *Technical report, Department of Computer Science, National Taiwan University, Taipei*, pp. 1–16, 2003.

[53] M. Anthony and P. L. Bartlett, *Neural network learning: Theoretical foundations*. Cambridge University Press, 2009.

[54] Y. A. LeCun, L. Bottou, G. B. Orr, and K.-R. Müller, "Efficient backprop," in *Neural networks: Tricks of the trade*, pp. 9–48, Springer, 2012.

[55] C. M. Bishop, *Neural networks for pattern recognition*. Oxford University Press, 1995.

[56] Y. Zhang and B. Wallace, "A sensitivity analysis of (and practitioners' guide to) convolutional neural networks for sentence classification," *arXiv preprint arXiv:1510.03820*, 2015.

[57] N. Srivastava, G. E. Hinton, A. Krizhevsky, I. Sutskever, and R. Salakhutdinov, "Dropout: a simple way to prevent neural networks from overfitting," *Journal of Machine Learning Research*, vol. 15, no. 1, pp. 1929–1958, 2014.

[58] S. Arlot, A. Celisse, *et al.*, "A survey of cross-validation procedures for model selection," *Statistics Surveys*, vol. 4, pp. 40–79, 2010.

[59] R. W. Homan, J. Herman, and P. Purdy, "Cerebral location of international 10–20 system electrode placement," *Electroencephalography and Clinical Neurophysiology*, vol. 66, no. 4, pp. 376–382, 1987.

[60] H. Tsunashima, K. Yanagisawa, and M. Iwadate, *Measurement of Brain Function Using Near-Infrared Spectroscopy (NIRS).* INTECH Open Access Publisher, 2012.

[61] M. Griebel, *Sparse grids and related approximation schemes for higher dimensional problems.* Citeseer, 2005.

[62] V. Nair and G. E. Hinton, "Rectified linear units improve restricted boltzmann machines," in *Proceedings of International Conference on Machine Learning (ICML-10)*, pp. 807–814, 2010.

[63] J. Bergstra and Y. Bengio, "Random search for hyper-parameter optimization," *Journal of Machine Learning Research*, vol. 13, no. Feb, pp. 281–305, 2012.

[64] D. Kingma and J. Ba, "Adam: A method for stochastic optimization," *arXiv preprint arXiv:1412.6980*, 2014.

Acknowledgments

Curriculum Vitae

Name   : Thanawin Trakoolwilaiwan

Date of Birth : November 08, 1992

E-mail   : thanawin.tra@gmail.com, thanawin@dgist.ac.kr

Educations

2005. 09. – 2017. 07. M.S. Information and Communication Engineering ,Daegu Gyeongbuk Institute of Science & Technology (DGIST), Daegu, South Korea

2011. 06. – 2015. 05. B.S. Biomedical Engineering, Mahidol University, Thailand

Professional Activities

2015. 08. 11 – 14   Thailand representative for 9th International Convention on Rehabilitation Engineering & Assistive Technology (i-CREATe 2015) at Nanyang Technological University, Singapore

2014. 04. – 2014. 08. Internship at Singapore Institute for Neurotechnology (SINAPSE), National University of Singapore, Singapore

Publications

1. **T. Trakoolwilaiwan**, K. Kim, and J.-W. Choi, "Classification Performance in Accuracy and Delay for Real-Time fNIRS-Based BCI System," *Annual International Conference of the IEEE Engineering in Medicine and Biology Society 2017 (EMBC'17)*, Jeju Island, South Korea, July 2017.

2. **T. Trakoolwilaiwan**, B. Behboodi, and J.-W. Choi, "Convolutional Neural Network for Functional Near-Infrared Spectroscopy in Brain-Computer Interface," Winter Conference, *Korea Information and Communications Society (KICS)*, (한국통신학회 동계학술대회), Jan 2017.

3. **T. Trakoolwilaiwan**, K. Kim, and J.-W. Choi, "Classification of Hand and Feet Motor Imagery Using Functional Near-Infrared Spectroscopy," *Annual International Conference of the IEEE Engineering in Medicine and Biology Society 2016 (EMBC'16)*, Orlando, United States, Aug 2016.

4. **T. Trakoolwilaiwan**, K. Kim, and J.-W. Choi, "The Feasibility of Using Wearable Functional Near-Infrared Spectroscopy (fNIRS) to Study Hemodynamic Response during Mental Arithmetic Task," Winter Conference, *Korea Information and Communications Society (KICS)*, (한국통신학회 동계학술대회), Jan 2016.